

Up to 256 GBd PAM Transmission Using Plasmonic Ring Resonator Modulator

Qian Hu, Robert Borkowski, Gregory Raybon

Nokia Bell Labs, 600 Mountain Ave, Murray Hill, NJ 07974, USA, qian.hu@nokia-bell-labs.com

Abstract We test plasmonic ring resonator modulator (RRM) for ultrafast optical intensity modulation and successfully demonstrate 256-GBd PAM-2, 186-GBd PAM-4, 168-GBd PAM-6, 160-GBd PAM-8 and 128-GBd PAM-12 transmission over 150-m standard single mode fiber. Record net bitrate 373-Gbit/s is achieved for RRM-based short-reach IM/DD link. ©2023 The Author(s)

Introduction

Co-packaging of photonic modules with electronic integrated circuits will bring significant improvements to power efficiency, bandwidth density and communication distance for computing and switching engines [1]. Silicon photonics (SiPh) leverages maturity of silicon CMOS process and enables fabrication of photonic and electronic devices on a single chip, therefore is an attractive solution for co-packaged optics [2]. Silicon modulators have advantages of small footprint, low insertion loss and can be easily fabricated. However, their modulation bandwidth and modulation efficiency are limited by the intrinsic properties of silicon. Using silicon modulators, the highest net bitrates achieved with intensity modulation and direct detection (IM/DD) were: 200 Gbit/s using a Mach-Zehnder modulator (MZM) [3] and 275 Gbit/s using a micro-ring modulator (MRM) [4], both assuming 20% forward error correction (FEC) overhead (OH).

To increase the modulation bandwidth and modulation efficiency, a metal-slot plasmonic waveguide filled with electro-optic (EO) material exhibiting high efficiency of Pockels effect can be seamlessly integrated on a standard SiPh platform [5]. Optical and electrical fields are tightly confined and overlap almost perfectly in the plasmonic waveguide of nano-scale width, making it possible to achieve sufficient phase shift already with a very short slot length (several microns) [6]. Optical intensity modulation is achieved by integrating plasmonic phase shifters

into conventional silicon waveguide structures: a Mach-Zehnder interferometer or a ring resonator. Thanks to the nanostructure of the metal slot, which results in a small RC constant, an ultrabroad EO bandwidth as high as 500 GHz have been reported [7]. Using a plasmonic MZM, high symbol rate optical IM: 222 GBd 2-level pulse amplitude modulation (PAM-2) [8], 156 GBd PAM-4 and 144 GBd PAM-8 [9] were experimentally demonstrated, resulting in net bitrates up to 363 Gbit/s. High insertion loss remains a major challenge faced by plasmonic MZMs, since plasmonic sections are inherently lossy. This can be circumvented by employing a ring resonator structure [10], where the cross-coupling efficiency of the resonator can be adjusted to reduce the loss originating from the plasmonic section. Lengths of coupler section and plasmonic section are jointly optimized at design phase to maximize the achievable optical modulation amplitude (OMA) [11]. An on-chip loss of only 1.5 dB has been reported with a plasmonic ring resonator modulator (RRM) [11]. Using a plasmonic RRM, transmission of 220 GBd PAM-2, 160 GBd PAM-4 and 136 GBd PAM-8 signals has been reported [11], yielding a net bitrate of 340 Gbit/s. Plasmonic MZMs and RRM clearly surpass their silicon-only counterparts in performance, as shown in the comparison in Fig. 1(a). In this work we explore the potential of plasmonic RRM to realize ultra-high-speed multi-level PAM in an optical IM/DD link for future data center interconnects. After

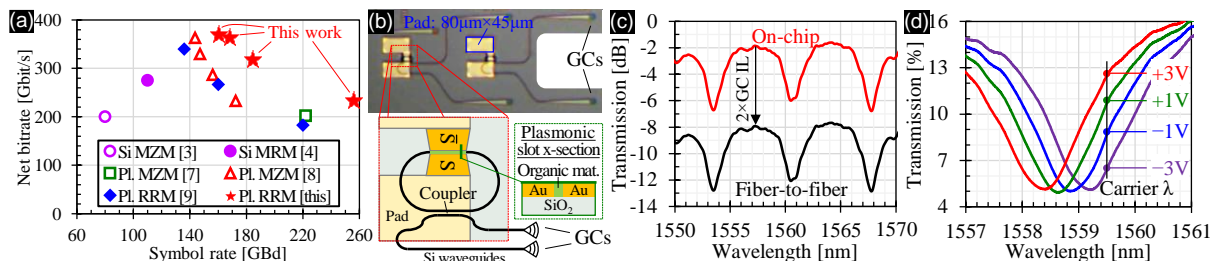


Fig. 1: (a) Comparison of this work to other record experiments based on SiPh (Si) and plasmonic (Pl.) technology. (b) Microscope photograph and schematic of the modulator (GC – grating coupler); insets show layout of the ring structure and the cross-section view of the plasmonic slot. (c) Transmission spectrum of the modulator under test calibrated for on-chip and fiber-to-fiber losses. (d) Spectrum shift under applied DC voltage and a drawing representing 4 level amplitude modulation.

150 m of C-band transmission, we successfully receive 256 GBd PAM-2 signal, as well as 160 GBd PAM-8 signal which has a net bitrate of 373 Gbit/s. These results are, to the best of our knowledge, the highest symbol rate and net bitrate demonstrated using plasmonic technology and/or micro-ring type modulator.

Modulator Under Test

Fig. 1(b) shows microscope photograph and schematic of the tested plasmonic RRM designed and fabricated by Polariton Technologies. The plasmonic slot is $7.5\ \mu\text{m}$ long and filled with electro-optic organic material, Lightwave Logic's Perkinamine™ chromophore series 3. The transmission spectrum under room temperature when no electrical signal is applied is shown in Fig. 1(c). Thermal stability of this modulator (due to environment temperature, optical input or electrical input) was investigated in [12] and was shown to outperform Si-only designs. The modulator provides a static extinction ratio (ER) of 5.2 dB (evaluated from the transmission peak wavelength at 1564.3 nm to the resonance wavelength at 1567.9 nm). The fiber-to-fiber insertion loss (IL) is 7.7 dB at 1564 nm, which includes 6.1 dB IL contributed by input and output grating couplers (GCs). After offsetting the GCs IL, the on-chip IL is 1.6 dB. Note that the optical bandwidth of the GCs constrains the operating wavelength to C-band, which restricts the transmission distance using IM/DD; nonetheless, O-band IM/DD transmission is possible with a modified design of the modulator. The modulator under test has a spectral tunability of 172 pm/V and an EO bandwidth higher than 110 GHz. When applying a voltage signal to the electrodes, multilevel intensity modulation is obtained as shown in Fig. 1(d), where spectral shift under various values of applied DC voltage is plotted.

Experimental Setup and Results

The plasmonic RRM is tested in an IM/DD setup shown in Fig. 2(a). 5 dBm continuous wave laser source emitting at 1559.5 nm is fed into the modulator. This wavelength was chosen to

demonstrate the best performance based on the maximum OMA consideration. The electrical signal generated from a 256 GSa/s arbitrary waveform generator (AWG) with a differential 5 Vpp swing. The electrical signal is applied to the modulator through a 110-GHz-bandwidth probe. The resulting optical signal is transmitted over a 150 m strand of a standard single-mode fiber. On the receiver side we use a preamplifier receiver equipped with an erbium-doped fiber amplifier (EDFA), followed by a 2 nm optical filter to emulate a wavelength demultiplexer and at the same time filter out-of-band amplified spontaneous emission (ASE) noise. The optical signal is detected by a 100 GHz *p-i-n* photodetector. The input power is kept at around 9 dBm to avoid signal-to-noise ratio degradation due to thermal noise. The resulting photocurrent is converted to voltage on the internal impedance of a real-time oscilloscope and sampled at 256 GSa/s.

Transmission performance is measured using PAM formats with 2, 4, 6, 8 and 12 levels. PAM-6 and -12 signals are obtained by time-interleaving amplitude of each dimension of, respectively, QAM-32 and QAM-128 constellations. Entropy of applied formats, H , is 1, 2, 2.5, 3 or 3.5 bit/symbol in ascending order of the number of modulation levels. PAM-2 signal is generated by the AWG at 1 Sa/symbol to obtain the highest possible symbol rate (256 GBd). No transmitter-side digital signal processing (DSP) is applied in this case. For other PAM formats, signals at various symbol rates R_s are digitally pulse-shaped by a raised-cosine filter with roll-off of 0.1 and resampled to 256 GSa/s. No pre-emphasis filter is applied at the transmitter side. Fig. 2(b) shows spectra of signals sampled by the real-time oscilloscope. The spectrum shape shows the end-to-end frequency response of the system; the modulator, which has more than 110 GHz EO bandwidth, has negligible impact on it. The receiver DSP consists of noise prefiltering, resampling, and a $T/2$ spaced simplified third-order Volterra nonlinear equalizer (VNLE), concatenated with a decision feedback equalizer

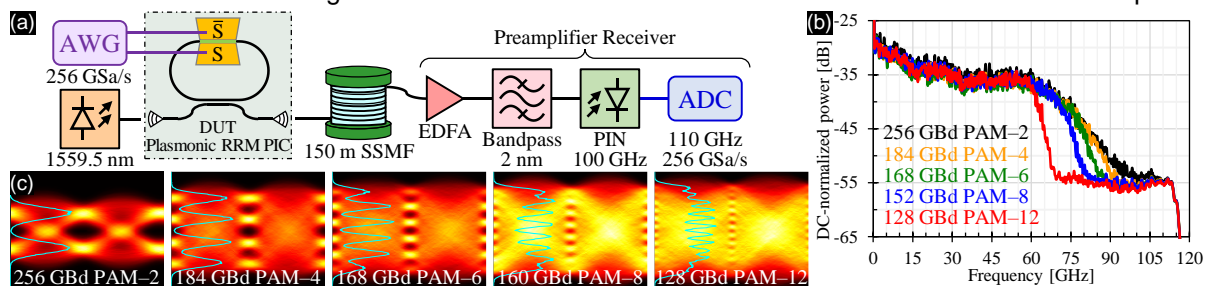


Fig. 2: (a) Experimental setup for performance evaluation of the plasmonic RRM; AWG – arbitrary waveform generator, DUT – device under test, RRM PIC – ring resonator modulator photonic integrated circuit, SSMF – standard single-mode fiber, EDFA – erbium-doped fiber amplifier, PIN – *p-i-n* photodiode, ADC – analog-to digital converter (real-time oscilloscope). (b) Spectra of ADC-sampled signals at various symbol rates and modulation orders. (c) Post-equalizer eye diagrams for signals under test.

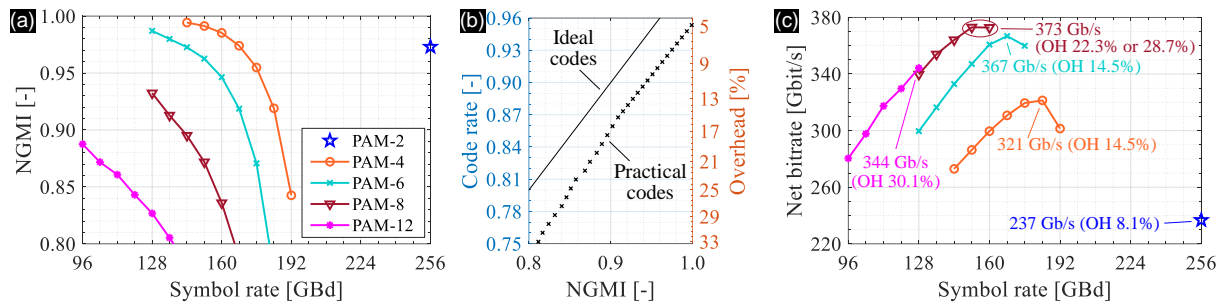


Fig. 3: (a) Normalized generalized mutual information (NGMI) as a function of symbol rate for PAM variants under test. (b) Overview of the codes used for net bitrate calculation (practical codes), as well as theoretical limit for ideal codes. (c) Calculated net bitrates as a function of symbol rate for PAM variants under test (same legend as in subfigure (a) applies).

(DFE). The VNLE uses linear terms originating from a span of 220 samples, while second and third order terms originate from a span of 50 samples. To limit the computational complexity, we only consider nonlinear terms produced from a span of at most 3 samples. The signal is resampled to 1 Sa/symbol at the output of the VNLE. Nine weights are used for DFE. Fig. 2(c) shows eye diagrams and histograms of the equalized signal for measured PAM formats at different symbol rates. For PAM-6 and -12 signals, two-dimensional constellation (QAM-32 or QAM-128) is reconstructed from two consecutive PAM symbols.

Fig. 3(a) shows normalized generalized mutual information (NGMI), computed from equalized symbols, as a function of symbol rate. To determine practically achievable net bitrates (bitrates after FEC OH removal) from the obtained NGMI values, a set of soft-decision and hard-decision concatenated FEC codes is considered [9]. Their code rates (left axis) and corresponding FEC overhead (nonlinear right axis) are plotted in Fig. 3(b) as a function of code NGMI thresholds. The information loss of considered practical codes is indicated by the vertical gap to the solid line of ideal codes. Post-FEC net bitrate is then computed as rHR_s , where r is the highest possible code rate in Fig. 3(b), which has NGMI threshold below the measured NGMI. As shown in Fig. 3(c), 256 GBd PAM-2 can achieve a net bitrate of 237 Gbit/s with 8.1% FEC overhead (OH). Higher net bitrate is achieved when increasing the number of modulation levels. For PAM-4 and -6 signals, net bitrates of 321 Gbit/s and 367 Gbit/s are achieved at 184 GBd and 168 GBd respectively, with 14.5% FEC OH. The highest net bitrate of 373 Gbit/s is obtained with PAM-8 signal either at 152 GBd with 22.3% FEC OH or at 160 GBd with 28.7% FEC OH. When further increasing the number of modulation levels to 12, the NGMI value decreases rapidly, and the required FEC OH exceeds 33.0% for symbol rates higher than 128 GBd. As a result, the highest net bitrate obtained with PAM-12 signal is lower than the

one obtained with PAM-6 or -8 signal. Using the plasmonic RRM, an optical IM/DD link with a net bitrate as high as 373 Gbit/s is successfully demonstrated.

Conclusions

Plasmonic ring resonator modulators (RRMs) features micron-scale footprint, ultrabroad EO bandwidth, high modulation efficiency and low on chip insertion loss. In this work, we used a plasmonic RRM to demonstrate high-symbol-rate multi-level optical intensity modulation in a short-reach IM/DD system and achieved the highest, up to now, symbol rate (256 GBd) and net bitrate (373 Gbit/s) for modulators based on plasmonic technology and/or ring resonator type. Our experimental demonstration shows great potential of plasmonic RRMs to enable compact and high-speed optical modulators for co-packaged datacenter optics.

Acknowledgements

The authors would like to thank Polariton Technologies and Lightwave Logic for their support and delivery of the plasmonic modulator and the organic material.

References

- [1] R. Mahajan, X. Li, J. Fryman, Z. Zhang, S. Nekkanty, P. Tadayon, J. Jaussi, S. Shumarayev, A. Agrawal, S. Jadhav, K. A. Singh, A. Alduino, S. Gujjula, C. -P. Chiu, T. Nordstog, K. J. Hosseini, S. Sane, N. Deshpande, K. Aygün, A. Sarkar, P. Dobriyal, S. Pothukuchi, V. A. Pogue, and D. Hui, "Co-Packaged Photonics for High Performance Computing: Status, Challenges and Opportunities," *Journal of Lightwave Technology*, vol. 40, no. 2, pp. 379–392, 2022, DOI: [10.1109/JLT.2021.3104725](https://doi.org/10.1109/JLT.2021.3104725).
- [2] S. Y. Siew, B. Li, F. Gao, H. Y. Zheng, W. Zhang, P. Guo, S. W. Xie, A. Song, B. Dong, L. W. Luo, C. Li, X. Luo, and G. -Q. Lo, "Review of Silicon Photonics Technology and Platform Development," *Journal of Lightwave Technology*, vol. 39, no. 13, pp. 4374–4389, 2021, DOI: [10.1109/JLT.2021.3066203](https://doi.org/10.1109/JLT.2021.3066203).
- [3] M. Jacques, Z. Xing, A. Samani, E. El-Fiky, X. Li, M. Xiang, S. Lessard, and D. V. Plant, "240 Gbit/s Silicon Photonic Mach-Zehnder Modulator Enabled by Two 2.3 Vpp Drivers," *Journal of Lightwave Technology*, vol. 38, no. 11, pp. 2877–2885, 2020, DOI: [10.1109/JLT.2020.2985589](https://doi.org/10.1109/JLT.2020.2985589).

- [4] D. W. U. Chan, X. Wu, A. P. T. Lau, C. Lu, and H. K. Tsang, "Single Lane 330 Gb/s Silicon Photonic Microring Modulator with sub $2 V_{pp}$ Driving Voltage," in *Proceedings OFC 2023*, San Diego, CA, USA, 2023, paper Th3B.4.
- [5] C. Koos, J. Leuthold, W. Freude, M. Kohl, L. Dalton, W. Bogaerts, A. L. Giesecke, M. Lauer mann, A. Melikyan, S. Koeber, S. Wolf, C. Weimann, S. Muehlbrandt, K. Koehnle, J. Pfeifle, W. Hartmann, Y. Kutuvantavida, S. Ummethala, R. Palmer, D. Korn, L. Alloatti, P. C. Schindler, D. L. Elder, T. Wahlbrink, and J. Bolten, "Silicon-Organic Hybrid (SOH) and Plasmonic-Organic Hybrid (POH) Integration," *Journal of Lightwave Technol.* vol. 34, no. 2, pp. 256–268, 2016, DOI: [10.1109/JLT.2015.2499763](https://doi.org/10.1109/JLT.2015.2499763).
- [6] W. Heni, Y. Fedoryshyn, B. Baeuerle, A. Josten, C. Hoessbacher, A. Messner, C. Haffner, T. Watanabe, Y. Salamin, U. Koch, D. L. Elder, L. R. Dalton, and J. Leuthold, "Plasmonic IQ modulators with attojoule per bit electrical energy consumption," *Nature Communications*, vol. 10, art. 1694, 2019, DOI: [10.1038/s41467-019-09724-7](https://doi.org/10.1038/s41467-019-09724-7).
- [7] M. Burla, C. Hoessbacher, W. Heni, C. Haffner, Y. Fedoryshyn, D. Werner, T. Watanabe, H. Massler, D. L. Elder, L. R. Dalton, and J. Leuthold, "500 GHz plasmonic Mach-Zehnder modulator enabling sub-THz microwave photonics," *APL Photonics*, vol. 4, no. 5, art. 056106, 2019, DOI: [10.1063/1.5086868](https://doi.org/10.1063/1.5086868).
- [8] W. Heni, B. Baeuerle, H. Mardoyan, F. Jorge, J. M. Estaran, A. Konczykowska, M. Riet, B. Duval, V. Nodjadjim, M. Goix, J.-Y. Dupuy, M. Destraz, C. Hoessbacher, Y. Fedoryshyn, H. Xu, D. L. Elder, L. R. Dalton, J. Renaudier, and J. Leuthold, "Ultra-High-Speed 2:1 Digital Selector and Plasmonic Modulator IM/DD Transmitter Operating at 222 GBaud for Intra-Datacenter Applications," *Journal of Lightwave Technology*, vol. 38, no. 9, pp. 2734–2739, 2020, DOI: [10.1109/JLT.2020.2972637](https://doi.org/10.1109/JLT.2020.2972637).
- [9] Q. Hu, R. Borkowski, Y. Lefevre, J. Cho, F. Buchali, R. Bonk, K. Schuh, E. De Leo, P. Habegger, M. Destraz, N. Del Medico, H. Duran, V. Tedaldi, C. Funck, Y. Fedoryshyn, J. Leuthold, W. Heni, B. Baeuerle, and C. Hoessbacher, "Ultrahigh-Net-Bitrate 363 Gbit/s PAM-8 and 279 Gbit/s Polybinary Optical Transmission Using Plasmonic Mach-Zehnder Modulator," *Journal of Lightwave Technology*, vol. 40, no. 10, pp. 3338–3346, 2022, DOI: [10.1109/JLT.2022.3172246](https://doi.org/10.1109/JLT.2022.3172246).
- [10] C. Haffner, D. Chelladurai, Y. Fedoryshyn, A. Josten, B. Baeuerle, W. Heni, T. Watanabe, T. Cui, B. Cheng, S. Saha, D. L. Elder, L. R. Dalton, A. Boltasseva, V. M. Shalaev, N. Kinsey, and J. Leuthold, "Low-loss plasmon-assisted electro-optic modulator," *Nature*, vol. 556, pp. 483–486, 2018, DOI: [10.1038/s41586-018-0031-4](https://doi.org/10.1038/s41586-018-0031-4).
- [11] M. Eppenberger, A. Messner, B. I. Bitachon, W. Heni, T. Blatter, P. Habegger, M. Destraz, E. De Leo, N. Meier, N. Del Medico, C. Hoessbacher, B. Baeuerle, and J. Leuthold "Plasmonic Micro-Racetrack Modulators," *Nature Photonics*, vol. 17, pp. 360–367, 2023, DOI: [10.1038/s41566-023-01161-9](https://doi.org/10.1038/s41566-023-01161-9).
- [12] M. Eppenberger, B. I. Bitachon, A. Messner, W. Heni, D. Moor, L. Kulmer, P. Habegger, M. Destraz, E. De Leo, N. Meier, N. D. Medico, C. Hoessbacher, B. Baeuerle, and J. Leuthold, "Enhanced Stability of Resonant Racetrack Plasmonic-Organic-Hybrid Modulators," in *Proceedings OFC 2022*, San Diego, CA, USA, 2022, paper Th3C.3, DOI: [10.1364/OFC.2022.Th3C.3](https://doi.org/10.1364/OFC.2022.Th3C.3).